

Prospects of LHC Higgs Physics at the end of Run III

Xin Chen^{1,2,3,a}, On behalf of the ATLAS and CMS Collaborations

¹Department of Physics, Tsinghua University, Beijing 100084, China

²Collaborative Innovation Center of Quantum Matter, Beijing 100084, China

³Center for High Energy Physics, Peking University, Beijing 100084, China

Abstract. The document is prepared for the LCWS2016 conference proceedings. The expected status of Higgs physics at the end of Run-3 is presented. The current Run-2 status is briefly reviewed, and the expected Higgs reach after the HL-LHC period is also summarized for some channels.

1 Introduction

The Large Hadron Collider (LHC) is taking data at $\sqrt{s} = 13$ TeV centre of mass energy. At the end of Run-2 (2018), an integrated luminosity of 150 fb^{-1} is expected, and at the end of Run-3, 300 fb^{-1} is expected, after which is the HL-LHC period until about 3 ab^{-1} of data is collected. There are two major detector upgrades happening after Run-2 and Run-3. Phase-I upgrade (2019-2020) prepares for an instantaneous luminosity of $2\text{-}3 \times 10^{34} \text{ cm}^{-2} \text{ s}^{-1}$. The production of detector parts for Phase-I has already started. The Phase-II upgrade (2024-2026) prepares for an instantaneous luminosity of $5\text{-}7.5 \times 10^{34} \text{ cm}^{-2} \text{ s}^{-1}$, and copes with an average pileup events of 140-200 per p - p collision. Phase-II is currently in the design and R&D stage. The major detector upgrades for the CMS and ATLAS experiments are outlined in Tab. 1:

Table 1. Major expected upgrades to the CMS and ATLAS detectors after the Phase-I and Phase-II upgrades.

	CMS	ATLAS
Tracking	Extended to $ \eta < 3.8$	Extended to $ \eta < 4.0$. All silicon
Calorimeter	Update all readout electronics. Timing in EM endcap (to reject pileup)	
Trigger	Tracking added at L1, larger bandwidth, finer granularity	
Muon	New chamber to complete $1.6 < \eta < 2.4$, muon tagger up to $ \eta < 3.0$	New endcap wheel to reject fake L1 muons (Phase-I)

The fiducial cross section measurement results with initial Run-2 data at $\sqrt{s} = 13$ TeV data are given in Tab. 2. The Higgs cross sections roughly scale with the center of mass energy, as displayed in Fig. 1 [1–5].

With about 10 times of the existing Run-1 data set, and larger Higgs cross sections, we are able to (1) precisely measure Higgs production and decay rates and couplings, (2) test the Higgs sector

^ae-mail: xin.chen@cern.ch

Table 2. The predicted and measured Higgs production fiducial cross sections with initial Run-2 $\sqrt{s} = 13$ TeV data at ATLAS and CMS [1, 2, 4, 5]. The luminosity used by ATLAS is 13.3 fb^{-1} (14.8 fb^{-1}) for $H \rightarrow \gamma\gamma$ ($H \rightarrow ZZ^* \rightarrow 4l$), and 12.9 fb^{-1} for CMS.

	$H \rightarrow \gamma\gamma$		$H \rightarrow ZZ^* \rightarrow 4l$	
	σ_{fid} (fb)	SM pred. (fb)	σ_{fid} (fb)	SM pred. (fb)
ATLAS	$43.2 \pm 14.9(\text{stat}) \pm 4.9(\text{sys})$	$62.8^{+3.4}_{-4.4}(\text{N3LO})$	$4.54^{+1.02}_{-0.90}$	$3.07^{+0.21}_{-0.25}$
CMS	$69^{+16}_{-22}(\text{stat})^{+8}_{-6}(\text{sys})$	73.8 ± 3.8	$2.29^{+0.74}_{-0.64}(\text{stat})^{+0.30}_{-0.23}(\text{sys})$	2.53 ± 0.13

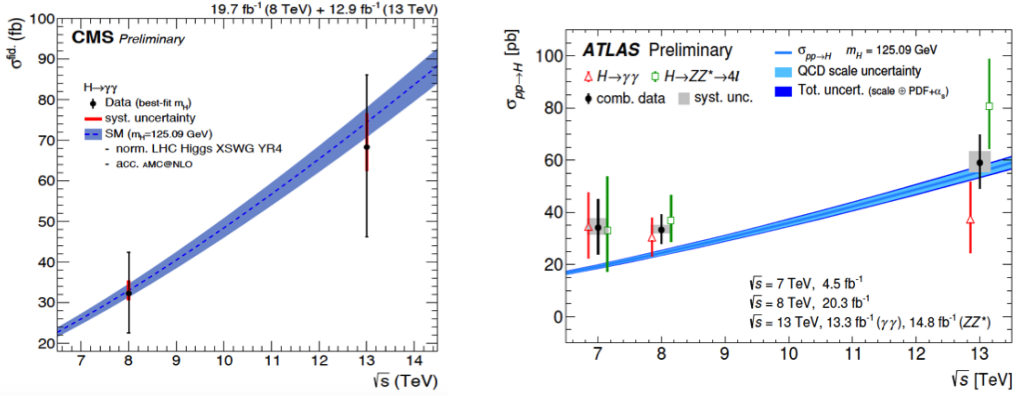


Figure 1. The measured cross sections of $H \rightarrow \gamma\gamma$ and $H \rightarrow ZZ^* \rightarrow 4l$ with initial Run-2 $\sqrt{s} = 13$ TeV data at CMS (left) [4] and ATLAS (right) [3].

and probe for Beyond Standard Model (BSM) such as Minimal Supersymmetric Standard Model (MSSM), the double Higgs production rate (order of few percent effects on Higgs couplings in most models), (3) search for rare/new/invisible decay modes, (4) use Effective Field Theory for the Higgs tensor structure study. Current theory errors on the Higgs gluon-gluon-Fusion (ggF) and Vector-Boson-Fusion (VBF) production cross sections are about 3-4% and 0.5% for the scale, 3% and 2% for $\text{PDF}+\alpha_s$, respectively [6]. The theory errors on the Higgs Branching Ratios (BR) are typically at 3-5%. Many projection results have particular assumptions made. The systematics can change and the analysis method can also improve. Projections for 300 fb^{-1} and 3 ab^{-1} (HL-LHC period) luminosities are given for some channels in this document. Physics projections for HL-LHC Higgs measurements are usually done in two ways:

- Parametrized detector performance. Event-generator level particles are smeared with detector performance parametrized from full simulation and reconstruction of upgraded HL-LHC detectors. Effects of pile-up are included for either $5 \times 10^{34} \text{ cm}^{-2} \text{ s}^{-1}$ (average 140 pile-up events which is the old default) or $7 \times 10^{34} \text{ cm}^{-2} \text{ s}^{-1}$ (average 200 pile-up events, current new setup). Analysis is mostly based on the existing 8 TeV results with simple re-optimization for higher luminosity.
- Extrapolation of Run-1 or Run-2 results. This means scaling signal and background to higher luminosities, correcting for different center-of-mass energy, assuming unchanged analysis (not re-optimized for higher luminosity) and the same detector performance as in Run-1/2 (some used corrections based on studies in the first approach).

For CMS, sometimes the projections are made with different systematics assumptions as listed in Tab. 3, which may appear in different projection plots and tables.

Table 3. The four different projection schemes at CMS with different assumptions of the systematics [12].

	systematics unchanged	exp. sys. scaled $1/\sqrt{\mathcal{L}}$	theo. sys. scaled 1/2	high PU effects
ECFA16 S1	✓	✗	✗	✗
ECFA16 S1+	✓	✗	✗	✓
ECFA16 S2	✗	✓	✓	✗
ECFA16 S2+	✗	✓	✓	✓

2 Projections for the signal strength and coupling factors

The projected uncertainty on the Higgs signal strength in different decays for ATLAS, and on the Higgs coupling to different particles for CMS, are shown in Fig. 2 [7, 8]. With larger statistics, the reduced coupling scale factors can be calculated to test the Higgs coupling dependence on the mass, as shown in Fig. 3 [7, 9]. The estimated precisions of such couplings with 3 ab^{-1} of data at ATLAS are about 3% for the W/Z boson, 7% for the muon, and 8-12% for the $t/b/\tau$ fermions.

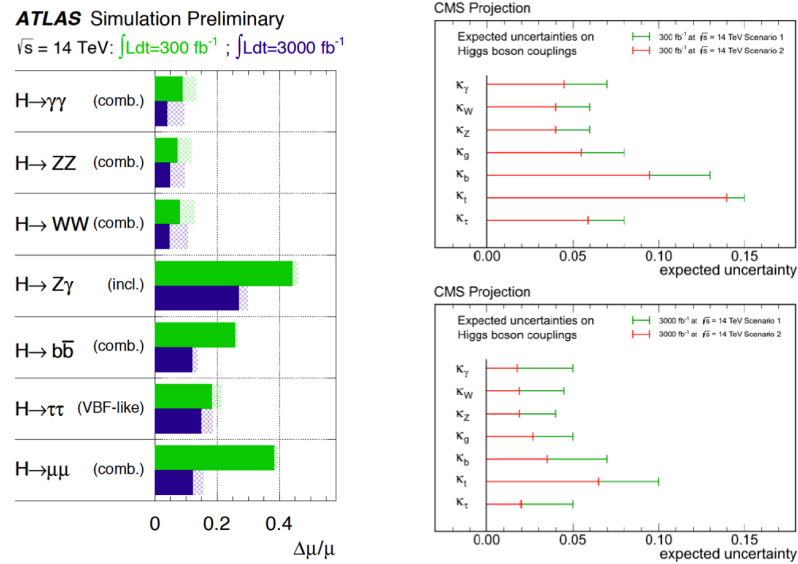


Figure 2. The projected uncertainty on the signal strength in different decays for ATLAS (left) [7], and on the Higgs coupling to different particles for CMS (right) [8], with 300 fb^{-1} and to 3 ab^{-1} of data.

3 Projections for $H \rightarrow ZZ^* \rightarrow 4l$

The $H \rightarrow ZZ^* \rightarrow 4l$ channel is relatively clean. With more data such as 3 ab^{-1} , the signal can be divided into VBF, VH, $t\bar{t}H$ and ggH categories, as shown in Fig. 4 [10, 11]. With 300 fb^{-1} of data,

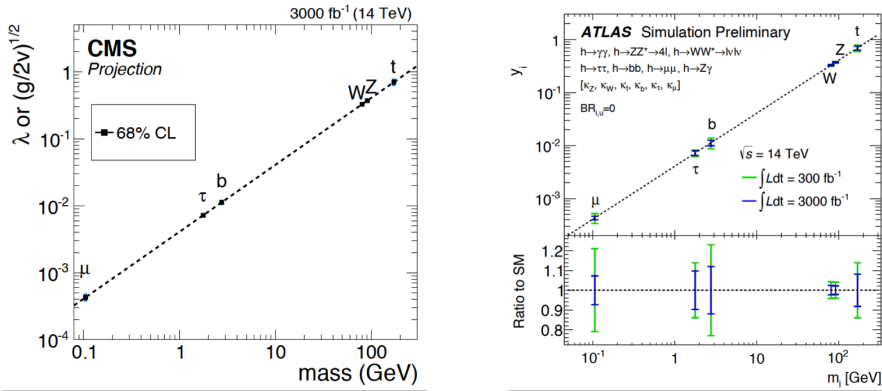


Figure 3. The reduced couplings of Higgs with different particles as a function of Higgs mass at CMS (left) [9] and ATLAS (right) [7].

the combined uncertainty on the signal strength, $\Delta\mu/\mu = 0.125$, can be achieved. The VBF region is almost background free, and a multivariate analysis, in this case the Boosted Decision Trees (BDT), can be used to further separate the ggF and VBF productions. The BDT distribution is also shown in Fig. 4, assuming an extended tracking coverage is implemented. With an average pileup events of 140 (200), $\Delta\mu/\mu = 0.17$ (0.18) and a signal significance of 7.7σ (7.2σ) can be reached. The Higgs mass distribution and the signal strengths in different production modes at CMS are shown in Fig. 5 [8, 12]. A $\Delta\mu/\mu$ of 5-10% can be achieved on the combined production of $H \rightarrow ZZ^* \rightarrow 4l$ (dominated by ggH) with 3 ab^{-1} at CMS. With abundant signal events, differential distributions such as the Higgs p_T can be also measured as shown in Fig. 6 [5, 12]. It is seen that going from 300 fb^{-1} to 3 ab^{-1} , the statistical and some systematic errors are greatly reduced (less than the theory errors at NLO).

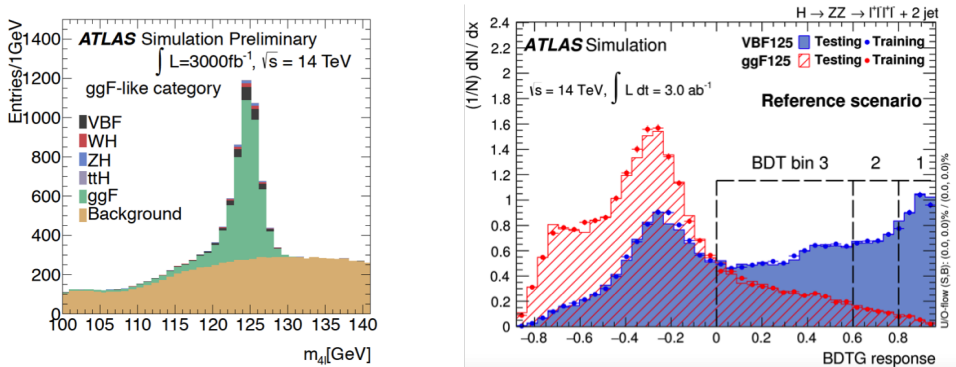


Figure 4. The Higgs mass distribution with different Higgs production contributions overlaid with 5 ab^{-1} (left) [10], and the BDT distribution in the VBF region to separate the ggF and VBF productions, in the $H \rightarrow ZZ^* \rightarrow 4l$ channel [11] at ATLAS.

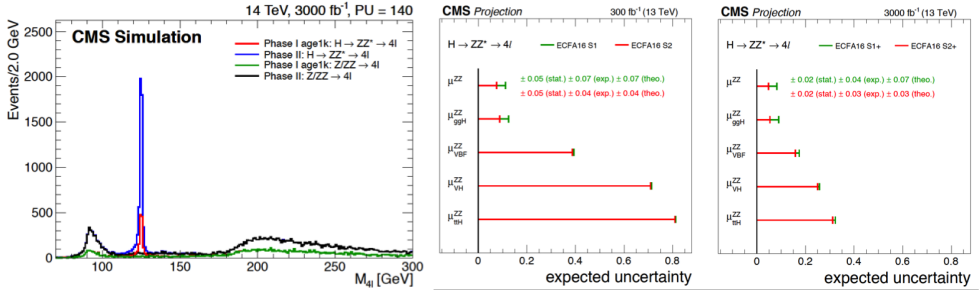


Figure 5. The Higgs mass distribution (left) and the signal strengths in different production modes with 300 fb^{-1} (middle) and 3 ab^{-1} (right) of data in the $H \rightarrow ZZ^* \rightarrow 4l$ channel at CMS [8, 12].

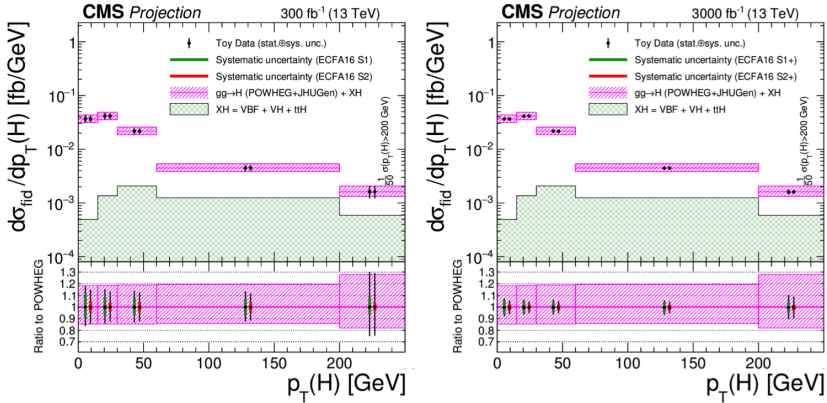


Figure 6. The differential distributions of the Higgs p_T after fiducial cuts with 300 fb^{-1} (left) and 3 ab^{-1} (right) of data in the $H \rightarrow ZZ^* \rightarrow 4l$ channel at CMS [5, 12].

The $H \rightarrow ZZ^* \rightarrow 4l$ channel can be also used to probe the anomalous tensor couplings in the following effective Lagrangian assuming spin-0 state of the Higgs:

$$\mathcal{L}_{HVV} \sim a_1 \frac{m_Z^2}{2} H Z^\mu Z_\mu - \frac{\kappa_1}{\Lambda_1^2} m_Z^2 H Z_\mu \square Z^\mu - \frac{1}{2} a_2 H Z^{\mu\nu} Z_{\mu\nu} - \frac{1}{2} a_3 H Z^{\mu\nu} \tilde{Z}_{\mu\nu}, \quad (1)$$

where the terms other than a_1 are BSM dimension-6 operators. Using the phase space distributions of the four leptons in the final state, limits on the coefficients from BSM terms can be set as in Fig. 7 [12], in which the f_{a_i} is defined as

$$f_{a_i} = \frac{|a_i|^2 \sigma_i}{\sum_j |a_j|^2 \sigma_j}, \quad (2)$$

where σ_i is the cross section from the i 'th term in Eq. 1. As the measurement is statistically limited, a big improvement in the sensitivity to the anomalous couplings with 3 ab^{-1} of data is expected.

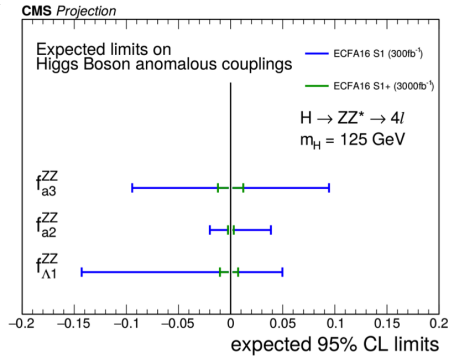


Figure 7. The expected limits on the anomalous Higgs couplings with 300 fb^{-1} and 3 ab^{-1} of data in the $H \rightarrow ZZ^* \rightarrow 4l$ channel at CMS [12].

4 Projections for $H \rightarrow \gamma\gamma$

The expected uncertainties for the Higgs fiducial cross section, and for the signal strength of different production modes in the $H \rightarrow \gamma\gamma$ decay are shown for CMS in Fig. 8 [12]. The fiducial cuts are defined at the generator level. The beam spot uncertainty in the beam direction is simulated to be about 5 cm with degraded vertex efficiency. The photon identification efficiency is degraded by 2.3% (10%) for the endcap+barrel (endcap+endcap) photons.

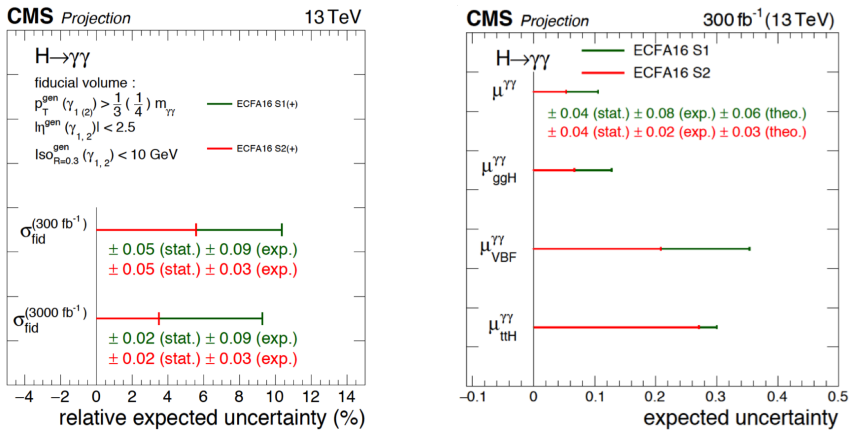


Figure 8. The expected uncertainties for the Higgs fiducial cross section (left), and for the signal strength of different production modes (right) in the $H \rightarrow \gamma\gamma$ decay at CMS [12].

5 Projections for $H \rightarrow Z\gamma$

The $H \rightarrow Z\gamma$ channel is very challenging due to the high level of SM background. With 300 fb^{-1} (3 ab^{-1}) of data, the expected signal significance is 2.3σ (3.9σ). However, this channel may be sensitive

to BSM through the loops. The $Z\gamma$ invariant mass distributions with $Z \rightarrow ee$ and $Z \rightarrow \mu\mu$ are shown in Fig. 9 for ATLAS [13].

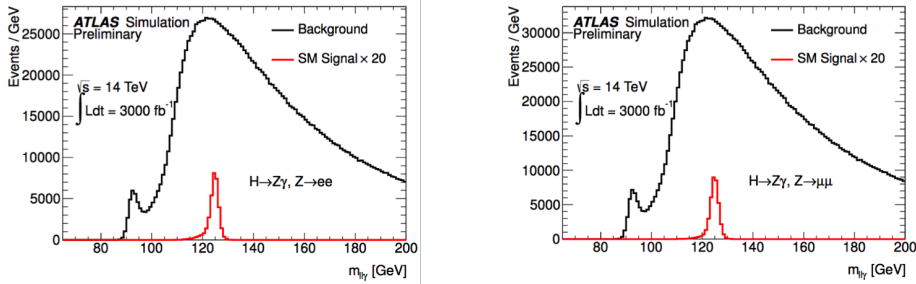


Figure 9. The $Z\gamma$ invariant mass distributions with $Z \rightarrow ee$ (left) and $Z \rightarrow \mu\mu$ (right) with $3 ab^{-1}$ of data at ATLAS [13].

6 Projections for $H \rightarrow J/\psi\gamma$

The $H \rightarrow J/\psi\gamma$ is sensitive to the Higgs coupling to charmed quarks. Using Run-1 data and the $J/\psi \rightarrow \mu^+\mu^-$ decay, an upper limit on the $BR(H \rightarrow J/\psi\gamma)$ has been set at 1.5×10^{-3} , while the SM prediction gives $BR(H \rightarrow J/\psi\gamma) = (2.9 \pm 0.2) \times 10^{-6}$. The $\mu^+\mu^-\gamma$ mass spectrum with $3 ab^{-1}$ of data is shown in Fig. 10 [14]. With $3 ab^{-1}$, about 3 signal events are expected out of 1700 background events. Expected limits with Multi-Variate-Analysis (MVA) with no background systematics are $BR(H \rightarrow J/\psi\gamma) < 44^{+19}_{-12} \times 10^{-6}$, and $\sigma(gg \rightarrow H) \times BR(H \rightarrow J/\psi\gamma) < 3.1^{+0.9}_{-1.3} fb$. Although the sensitivity is not great, BSM physics can potentially enhance the rate and give an observable signal.

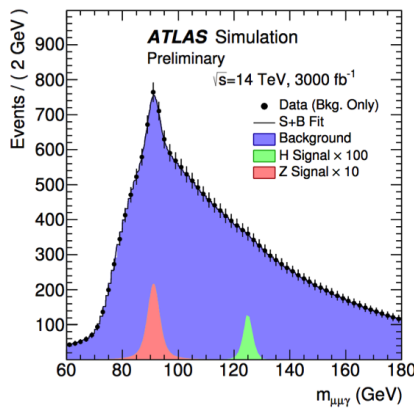


Figure 10. The expected $\mu^+\mu^-\gamma$ mass spectrum in the $H \rightarrow J/\psi\gamma$ channel with $3 ab^{-1}$ of data at ATLAS [14].

7 Projections for the Higgs width

The Higgs width can be measured by the interference between the triangle and box diagrams in the $gg \rightarrow VV$ process, as illustrated in Fig. 11. With the $H \rightarrow ZZ \rightarrow 4l$ final state, the 4-lepton mass shape

and the Matrix Element (ME) for each event can be used to discriminate the signal from background. Fig. 11 also shows the 4-lepton mass and ME distributions [15]. When combined with the on-shell measurements of the Higgs, the Higgs width can be estimated. In Run-1 with the three decays of $ZZ \rightarrow 4l$, $ZZ \rightarrow 2l2\nu$ and $WW \rightarrow e\nu\mu\nu$, upper limits of $\mu_{\text{offshell}} < 6.2$ (8.1), and $\Gamma_H/\Gamma_H^{SM} < 5.5$ (8.0) for the observation (expectation), were obtained. With 3 ab^{-1} , the precision can be improved to $\mu_{\text{offshell}} = 1.00_{-0.50}^{0.43}$ and $\Gamma_H = 4.2_{-2.1}^{+1.5} \text{ MeV}$ (statistical + systematic errors).

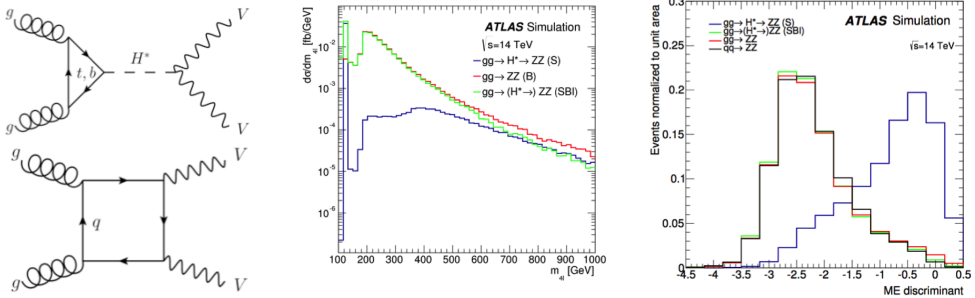


Figure 11. The Feynman diagrams for the $gg \rightarrow VV$ process (left), the distributions of the 4-lepton mass (middle) and the ME (right) in the $ZZ \rightarrow 4l$ final state at ATLAS [15].

8 Projections for $H \rightarrow \mu\mu$

The $H \rightarrow \mu\mu$ channel is very challenging because of the low BR. In Fig. 12 [8, 10], the dimuon mass spectrum with 3 ab^{-1} of data, the dimuon mass resolution for different detector and pileup conditions, and the dimuon mass in the $t\bar{t}H$ associated production are given. The sharpness of the dimuon mass is crucial for both ATLAS and CMS. The $H\mu\mu$ coupling can be measured to a precision of 8-20% with 3 ab^{-1} . In the $t\bar{t}H$, $H \rightarrow \mu\mu$ channel, about 33 signal events can be selected out of about 22 background events, and with 300 fb^{-1} , $\Delta\mu/\mu = 46\%$ and a signal significance of 2.3σ can be reached.

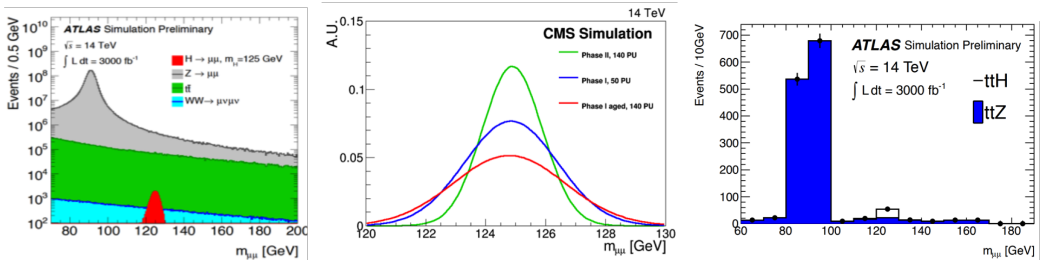


Figure 12. The dimuon mass spectrum with 3 ab^{-1} of data for ATLAS (left), the dimuon mass resolution for different detector and pileup conditions for CMS (middle), and the dimuon mass in the $t\bar{t}H$ associated production for ATLAS (right) [8, 10].

9 Projections for the double Higgs production

The Higgs self-coupling is measured with the double Higgs production. The relevant Feynman diagrams are shown in Fig. 13. For the non-resonant SM double Higgs production, the triangle and

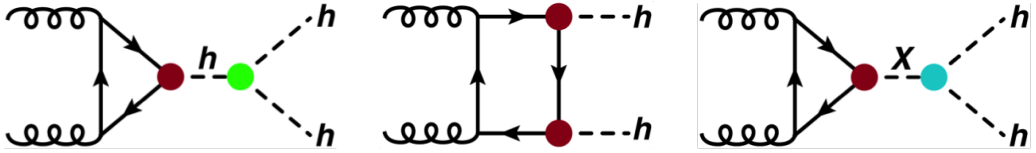


Figure 13. The SM (left, middle) and BSM (right) diagrams that contribute to the double Higgs production at the LHC [12].

box diagrams have negative interference, and the NNLO+NNLL prediction of the cross section is $\sigma = 33.45$ fb at 13 TeV. The invariant mass of $\gamma\gamma$ and $b\bar{b}$ in the $HH \rightarrow b\bar{b}\tau\tau$ channel, and of the $b\bar{b}$ and $\gamma\gamma$ in the $HH \rightarrow b\bar{b}\gamma\gamma$ channel with $3 ab^{-1}$ of data at ATLAS are shown in Fig. 14 [16–19]. The signal significances for $HH \rightarrow b\bar{b}\gamma\gamma$, $HH \rightarrow b\bar{b}\tau\tau$ and $t\bar{t}HH \rightarrow t\bar{t}b\bar{b}b\bar{b}$ are 1.3σ , 0.6σ and 0.35σ respectively. The 95% CL interval for the Higgs quartic coupling constant is $-1.3 < \lambda/\lambda_{SM} < 8.7$ ($-7.4 < \lambda/\lambda_{SM} < 14$) in the $HH \rightarrow b\bar{b}\gamma\gamma$ ($HH \rightarrow b\bar{b}b\bar{b}$) channel. The expected uncertainties on the signal strength in different double Higgs decay modes from CMS are shown in Fig. 15 [12], and the upper limits on the signal strength are also listed in Tab. 4 [12]. Sensitivity for the SM double Higgs production is still quite limited; anyway several BSM models can be excluded.

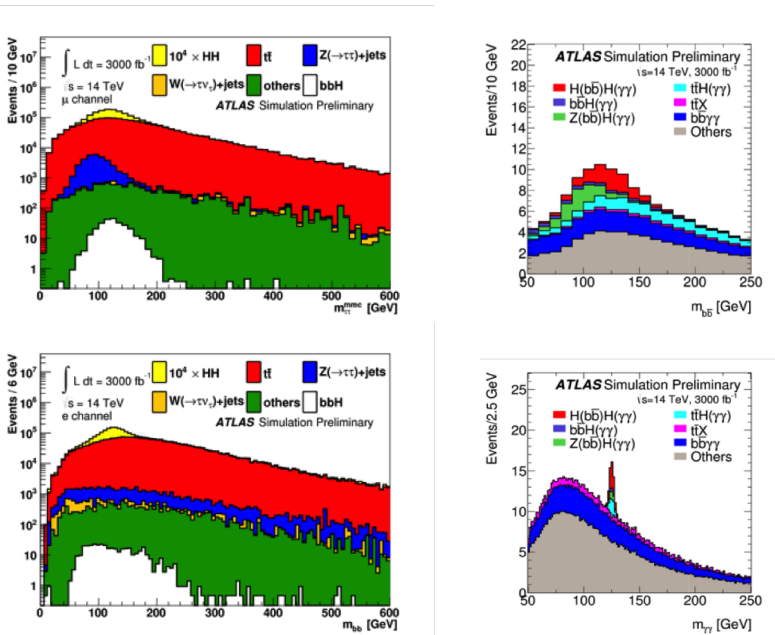


Figure 14. The invariant mass of $\gamma\gamma$ and $b\bar{b}$ in the $HH \rightarrow b\bar{b}\tau\tau$ channel (left column), and of the $b\bar{b}$ and $\gamma\gamma$ pairs in the $HH \rightarrow b\bar{b}\gamma\gamma$ channel (right column) with $3 ab^{-1}$ of data at ATLAS [16–19].

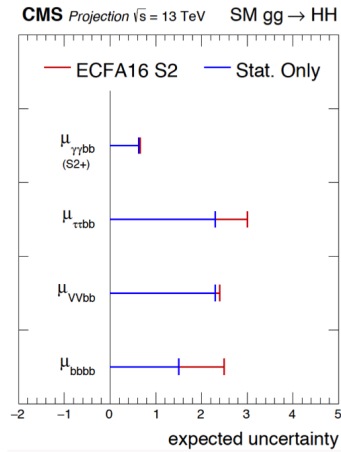


Figure 15. The expected uncertainties on the signal strength in different double Higgs decay modes with 3 ab^{-1} of data at CMS [12].

Table 4. The expected upper limits on the signal strength of the double Higgs production signal in different decay modes with 3 ab^{-1} of data at CMS [12].

Channel	Median expected limits in μ_r			Z-value			Uncertainty as fraction of $\mu_r = 1$		
	ECFA16		Stat. Only	ECFA16		Stat. Only	ECFA16		Stat. Only
	S1	S2		S1	S2		S1	S2	
$gg \rightarrow HH \rightarrow \gamma\gamma bb$ (S1+/S2+)	1.3	1.3	1.3	1.6	1.6	1.6	0.64	0.64	0.64
$gg \rightarrow HH \rightarrow \tau\tau bb$	7.4	5.2	3.9	0.28	0.39	0.53	3.7	2.6	1.9
$gg \rightarrow HH \rightarrow VV bb$		4.8	4.6		0.45	0.47		2.4	2.3
$gg \rightarrow HH \rightarrow bbbb$		7.0	2.9		0.39	0.67		2.5	1.5

10 Projections for MSSM $H \rightarrow \tau\tau$

In MSSM, there are five Higgs scalars, namely h , A , H and H^\pm . To be compatible with a 125 GeV Higgs, usually two scenarios are considered:

- hMSSM scenario: the measured value of 125 GeV can be used to predict masses and decay branching ratios of the other Higgs bosons.
- $m_h^{\text{mod+}}$ scenario: the lightest CP-even Higgs is assigned to be the 125 GeV boson.

The expected exclusion region in the m_A - $\tan\beta$ plane in the $m_h^{\text{mod+}}$ scenario for the $\phi \rightarrow \tau\tau$ decay at CMS is shown in Fig. 16 [12].

11 Projections for VBF $H \rightarrow$ invisible

The Higgs can decay to dark matter particles such as the neutralinos leading to large Missing E_T (MET) events. To select these events, MET triggers are required, and the VBF region with large m_{jj} and $\Delta\eta_{jj}$ cuts are investigated. Dedicated $Z \rightarrow ll$ and $W \rightarrow lv$ control regions are available to check the background from single vector boson processes. The VBF channel is found to be more powerful

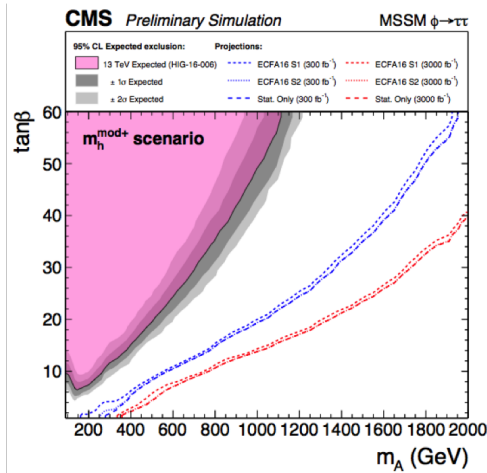


Figure 16. The expected exclusion region in the m_A - $\tan\beta$ plane in the $m_h^{\text{mod}+}$ scenario for the MSSM $\phi \rightarrow \tau\tau$ decay at CMS [12].

than the VH, $H \rightarrow$ invisible channel. With Run-1 data, the limit of $\text{BR}(H \rightarrow \text{invisible}) < 0.28$ (0.31) was obtained for the observation (expectation) from ATLAS [20]. The projected limits with the VBF production as a function of integrated luminosity from CMS are shown in Fig. 17 [12].

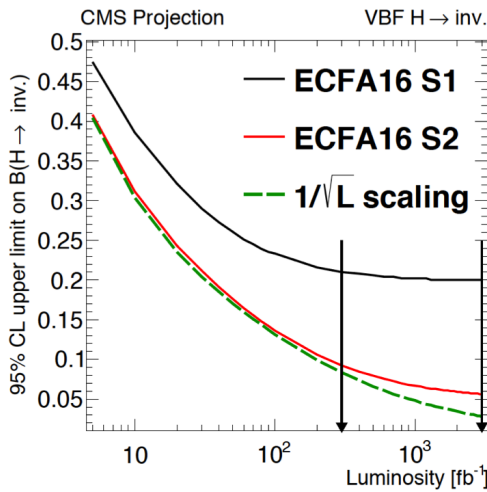


Figure 17. The projected limits on $H \rightarrow$ invisible BR with the VBF production as a function of integrated luminosity from CMS [12].

12 Conclusion

With a successful startup of LHC Run-2, both CMS and ATLAS are fully engaged in the 13 TeV centre of mass energy running. To exploit at best the LHC upgrade (Run III and HL-LHC), both experiments have to cope with the challenges of increased pileup rates with dedicated upgrades to the detectors. At the end of Run 3 with $300 fb^{-1}$, the Higgs couplings can be measured to 10-20%. At the end of HL-LHC with $3 ab^{-1}$ of data, the precision on the couplings can improve to about 5-10%, and statistically limited measurements, like the differential Higgs distributions and test for Higgs tensor couplings, can be significantly improved. Rare Higgs decays can be probed as well. For example, the $H \rightarrow \mu\mu$ channel can reach $< 20\%$ precision, and the sensitivity for the anomalous $H \rightarrow J/\psi\gamma$ decay at $10\times SM$ level can be achieved. The Higgs self-coupling via double Higgs productions can be searched for, although is still quite challenging. Indirect search for BSM through the Higgs width, and direct search for new signatures such as $H \rightarrow$ invisible and the MSSM Higgs will make tighter tests of the theory. Higgs precision physics is one of the main motivations and design considerations for the HL-LHC and experiments programs.

References

- [1] ATLAS Collaboration, ATLAS-CONF-2016-067.
- [2] ATLAS Collaboration, ATLAS-CONF-2016-079.
- [3] ATLAS Collaboration, ATLAS-CONF-2016-081.
- [4] CMS Collaboration, CMS-PAS-HIG-16-020.
- [5] CMS Collaboration, CMS-PAS-HIG-16-033.
- [6] D. de Florian et al., arXiv:1610.07922.
- [7] ATLAS Collaboration, ATL-PHYS-PUB-2014-016.
- [8] CMS Collaboration, LHCC-P-008.
- [9] CMS Collaboration, LHCC-G-165.
- [10] ATLAS Collaboration, ATL-PHYS-PUB-2013-014.
- [11] ATLAS Collaboration, ATL-PHYS-PUB-2016-008.
- [12] CMS Collaboration, CMS DP-2016/064.
- [13] ATLAS Collaboration, ATL-PHYS-PUB-2014-006.
- [14] ATLAS Collaboration, ATL-PHYS-PUB-2015-043.
- [15] ATLAS Collaboration, ATL-PHYS-PUB-2015-024.
- [16] ATLAS Collaboration, ATL-PHYS-PUB-2014-019.
- [17] ATLAS Collaboration, ATL-PHYS-PUB-2015-046.
- [18] ATLAS Collaboration, ATL-PHYS-PUB-2016-023.
- [19] ATLAS Collaboration, ATL-PHYS-PUB-2016-024.
- [20] ATLAS Collaboration, JHEP 01 (2016) 172.